Zhao *et al. Satellite Navigation* (2023) 4:22
https://doi.org/10.1186/s43020-023-00112-7

Satellite Navigation
https://satellite-navigation.springeropen.com/

ORIGINAL ARTICLE

Open Access

A new inter-system double-difference RTK model applicable to both overlapping and non-overlapping signal frequencies

Wenhao Zhao[1,2], Genyou Liu[1*], Ming Gao[3], Bo Zhang[1,2], Shengjun Hu[1,2] and Minghui Lyu[1,2]

Abstract

Aiming at the problem that the traditional inter-system double-difference model is not suitable for non-overlapping signal frequencies, we propose a new inter-system double-difference model with single difference ambiguity estimation, which can be applied for both overlapping and non-overlapping signal frequencies. The single difference ambiguities of all satellites and Differential Inter-System Biases (DISB) are first estimated, and the intra-system double difference ambiguities, which have integer characteristics, are then fixed. After the ambiguities are successfully fixed, high-precision coordinates and DISB can be obtained with a constructed transformation matrix. The model effectively avoids the DISB parameter filtering discontinuity caused by the reference satellite transformation and the low precision of the reference satellite single difference ambiguity calculated with the code. A zero-baseline using multiple types of receivers is selected to verify the stability of the estimated DISB. Three baselines with different lengths are selected to assess the positioning performance of the model. The ionospheric-fixed and ionospheric-float models are used for short and medium-long baselines, respectively. The results show that the Differential Inter-System Code Biases (DISCB) and Differential Inter-System Phase Biases (DISPB) have good stability regardless of the receivers type and the signal frequency used and can be calibrated to enhance the strength of the positioning model. The positioning results with three baselines of different lengths show that the proposed inter-system double-difference model can improve the positioning accuracy by 6–22% compared with the intra-system double-difference model which selects the reference satellite independently for each system. The Time to First Fix (TTFF) of the two medium-long baselines is reduced by 30% and 29%, respectively.

Keywords Global navigation satellite systems, Real-time, Inter-system biases, Ambiguity resolution, Medium-long baselines

Introduction

Global Navigation Satellite System (GNSS) has entered a multi-constellation and multi-frequency era (Tao et al., 2022), which can provide more powerful positioning services, but also increases the complexity of data processing (Teunissen & Khodabandeh, 2022). Compared with a single system, multiple systems can position with higher accuracy and reliability (Xiao et al., 2020). Similarly, multi-frequency data can also improve the positioning performance (Wu et al., 2022). More and more attention has been paid to the high-precision positioning technology of multi-frequency and multi-systems.

*Correspondence:
Genyou Liu
liugy@whigg.ac.cn
[1] State Key Laboratory of Geodesy and Earth's Dynamics, Innovation Academy for Precision Measurement Science and Technology, Chinese Academy of Sciences, Wuhan 430077, China
[2] University of Chinese Academy of Sciences, Beijing 100049, China
[3] Aerospace Information Research Institute, Chinese Academy of Sciences, Beijing 100094, China

Double-difference Real-Time Kinematic (RTK) is a commonly used model of high-precision positioning. In multi-system RTK positioning, each system usually selects its reference satellite, which is called the intra-system double difference model (Robert Odolinski & Teunissen, 2020). Compared with the intra-system double difference model, the inter-system double difference model uses a common reference satellite for all the systems, resulting in more observations, which can theoretically enhance the strength of the model and improve the positioning accuracy (Chen et al., 2021; Paziewski & Wielgosz, 2015). The inter-system double-difference model must consider the effect of Differential Inter-System Biases (DISB). DISB is caused by different systems related to the receiver hardware delay (Paziewski & Wielgosz, 2015).

Odijk and Teunissen (Odijk & Teunissen, 2013) analyzed the stability of DISB, and the results show that DISB is stable for the overlapping signal frequency regardless of the receiver types. The influence of DISB can be ignored when the receiver type is the same. Gao et al. (Gao et al., 2018) analyzed the DISB characteristic for the non-overlapping signal frequency, and the results show that the DISB for non-overlapping frequency cannot be ignored, but has good stability independent of receiver types.

Inter-system RTK models are usually divided into two types: the DISB-float and DISB-fixed, according to the ways of handling DISB (Zhao et al., 2022). The DISB-float model estimates the DISB parameters together with the receiver coordinates and ambiguity parameters. In the single epoch mode, the DISB-float model has the same model strength as the intra-system RTK model (Wu et al., 2018). In the multi-epoch mode, the stability of the DISB parameter can be used to improve the model strength and positioning accuracy. Odijk and Teunissen (Odijk & Teunissen, 2013) used the method of parameter renormalization to integrate the double difference ambiguity between reference satellites into the DISB parameters, and the influence of the reference satellite transformation must be considered in the multi-epoch mode. This method is suitable for overlapping signal frequencies, and the influence of the single difference ambiguity of the reference satellite must be considered for non-overlapping frequencies (Jia et al., 2019). Mi et al. (2019) proposed an inter-system RTK model based on a single difference model, which can be adapted for non-overlapping signal frequencies. Both single difference and double difference DISB-float model use the feature of stable multi-epoch DISB to improve the positioning accuracy.

The DISB-fixed model uses a priori DISB to correct the model, and higher model strength and positioning accuracy can also be obtained in the single-epoch mode. Tian et al. (2017) used particle filter to estimate DISB based on the DISB-fixed model, which does not require a priori DISB. Sui et al. (2018) used particle swarm optimization algorithm to search DISB based on the DISB-fixed model, which does not require a priori DISB. The principle of these two methods is to obtain the DISB parameter with the largest ratio value as the true value (Rui Shang et al., 2021a, 2021b), which creates the DISB half-cycle problem (Tian et al., 2017). The half-cycle problem seriously affects the stability of the estimated DISB parameters and the positioning accuracy. Zhao et al. (2021) proposed a method to effectively avoid the Inter-System Biases (ISB) half-cycle problem by transforming the search space of ISB.

In this contribution, we propose a new inter-system double difference RTK model with single difference ambiguity estimation that can be applied for both overlapping and non-overlapping signal frequencies. In this model, a satellite among multiple systems is selected as the common reference satellite to form the inter-system double difference observation equation. Compared with the traditional intra-system double difference RTK model, the number of observation equations is increased, and theoretically higher positioning accuracy can be obtained. Compared with other inter-system double difference models suitable for non-overlapping signal frequencies, the proposed model does not need to calculate the single difference ambiguity of the reference satellite in advance. Because the model estimates the single difference ambiguity, the influence of the reference satellite transformation is not considered. Because of the existence of DISB, the inter-system double difference ambiguity no longer has integer characteristics, so we form the intra-system double difference ambiguity which has integer characteristics. After the ambiguity is successfully fixed, the high-precision coordinates and DISB can be obtained with a constructed transformation matrix. Benefiting from the stability of the DISB parameters, with the multi-epoch observations the model can achieve better positioning results than the traditional inter-system model. We first evaluate the stability of DISB using this model, which is a prerequisite for precise positioning. We finally use this model with the ionospheric-fixed and ionospheric-float to test the positioning performance with the baselines of different lengths.

In the next section, a new inter-system double-difference model with single difference ambiguity estimation is introduced. The model is divided into the ionospheric-fixed model and ionospheric-float model according to different ionospheric processing modes. Subsequently, we analyze the DISB stability of dual- frequencies signals for Global Positioning System (GPS), BeiDou Navigation Satellite System (BDS), Galileo navigation satellite system

(Galileo), which contains overlapping and non-overlapping signal frequencies, and multiple types of receivers are also considered. Finally, we test the positioning performance with the proposed model using three baselines of different lengths, a short baseline and two medium-long baselines.

Methods

This section first introduces the proposed inter-system double-difference model. The model can be extended to multiple systems and multiple frequencies, but only if these frequencies are allowed to be combined (Tian et al., 2018). In addition, to make the model applicable to the baselines of different lengths, we also introduce the ionospheric-fixed and ionospheric-float models.

Ionospheric-fixed inter-system double-differenced model

The double difference RTK model can eliminate the effects of the ionosphere and troposphere for short baselines (Odolinski et al., 2014). The ionospheric-fixed single-differenced observation equations are formulated as

$$\begin{cases} \Delta P_{br,i}^{s_A} = \Delta\rho_{br}^{s_A} + \Delta \mathrm{d}t_{br} + \Delta d_{br,i}^{A} + \Delta e \\ \Delta\varphi_{br,i}^{s_A} = \Delta\rho_{br}^{s_A} + \Delta \mathrm{d}t_{br} + \lambda_i\left(\Delta\Phi_{br,i} + \Delta\delta_{br,i}^{A} + \Delta N_{br,i}^{s_A}\right) + \Delta\varepsilon \end{cases} \tag{1}$$

where b and r represent two different Global Navigation Satellite System (GNSS) receivers, S represents GNSS satellite, A represents a satellite system, i represents frequency, ΔP and $\Delta\varphi$ represent the observed single difference code and single difference phase in meters, and λ represents wavelength. We further have the single differences between receivers $\Delta\rho_{br}^{s_A}$ (distance), $\Delta \mathrm{d}t_{br}$ (clock error), $\Delta d_{br,i}^{A}$ (code hardware delay), $\Delta\Phi_{br,i}$ (initial phase bias), $\Delta\delta_{br,i}^{A}$ (carrier phase hardware delay), $\Delta N_{br,i}^{s_A}$ (integer ambiguity), and Δe and $\Delta\varepsilon$ represent the code and phase measurement errors.

A satellite is selected as the reference satellite for both systems, and the intra-system and inter-system double-differenced observation equations are formed simultaneously. The ionospheric-fixed inter-system double-differenced observation equations are formulated as follows:

$$\begin{cases} \Delta\nabla P_{br,i}^{1_A s_A} = \Delta\nabla\rho_{br}^{1_A s_A} + \Delta\nabla e \\ \Delta\nabla\varphi_{br,i}^{1_A s_A} = \Delta\nabla\rho_{br}^{1_A s_A} + \lambda_i\Delta N_{br,i}^{s_A} - \lambda_i\Delta N_{br,i}^{1_A} + \Delta\nabla\varepsilon \\ \Delta\nabla P_{br,ij}^{1_A s_B} = \Delta\nabla\rho_{br}^{1_A s_B} + \Delta d_{br,j}^{B} - \Delta d_{br,i}^{A} + \Delta\nabla e \\ \Delta\nabla\varphi_{br,ij}^{1_A s_B} = \Delta\nabla\rho_{br}^{1_A s_B} + \left(\lambda_j\Delta\Phi_{br,j} - \lambda_i\Delta\Phi_{br,i}\right) + \left(\lambda_j\Delta\delta_{br,j}^{B} - \lambda_i\Delta\delta_{br,i}^{A}\right) \\ \qquad\qquad + \lambda_j\Delta N_{br,j}^{s_B} - \lambda_i\Delta N_{br,i}^{1_A} + \Delta\nabla\varepsilon \end{cases} \tag{2}$$

where $\Delta\nabla$ is the double-difference operator, 1_A and s_A represent the reference and non-reference satellite of system A, respectively. The hardware delay and other parameters are reorganized as follows:

$$\begin{cases} \Delta d_{br,j}^{B} - \Delta d_{br,i}^{A} = b_{\mathrm{DISCB}} \\ \left(\lambda_j\Delta\Phi_{br,j} - \lambda_i\Delta\Phi_{br,i}\right) + \left(\lambda_j\Delta\delta_{br,j}^{B} - \lambda_i\Delta\delta_{br,i}^{A}\right) = \lambda_j b_{\mathrm{DISPB}} \end{cases} \tag{3}$$

where b_{DISCB} and b_{DISPB} represent Differential Inter-System Code Biases (DISCB) and Differential Inter-System Phase Biases (DISPB), respectively. The state vector is rearranged as follows:

$$\boldsymbol{X} = \left(x\ y\ z\ b_{\mathrm{DISPB}}\ b_{\mathrm{DISCB}}\ \Delta N_{br,i}^{s_A}\ \Delta N_{br,j}^{s_B}\right) \tag{4}$$

Since the single difference ambiguity and the DISB parameter are linearly dependent, this equation is rank deficient. A feasible approach is to use the S-basis method to reorganize the linearly dependent parameters (Khodabandeh & Teunissen, 2016; Odijk et al., 2016). In this paper we assign an approximate initial value and an approximate initial variance to all the state parameters (Takasu & Yasuda, 2009). It is important to point out that only at the initial epoch, the value and variance of the state vector need to be assigned. After obtaining the initial values and variances of all the states, we can use the Kalman filter to update measurements to obtain the float solutions of the state parameters. Although we obtain float solutions for the parameters, there is still a linear dependence between them. We need constructing a transformation matrix to reorganize the linearly dependent parameters. This is equivalent to the S-basis method. The difference is that the S-basis method reorganizes the parameters before parameter estimation, while the method in this paper reorganizes the parameters after parameter estimation. Due to the existence of DISB, the single difference ambiguity is not directly composed of the inter-system double difference ambiguities. We can construct a transformation matrix to convert the single difference ambiguity into the intra-system double difference ambiguity. This is because the intra-system

ambiguity parameters are not affected by DISB and the intra-system double difference ambiguity still has the integer characteristics. The transformation matrix D is constructed as follows:

$$\begin{cases} \boldsymbol{D} = \begin{bmatrix} \boldsymbol{D}_A & \boldsymbol{O} \\ \boldsymbol{O} & \boldsymbol{D}_B \end{bmatrix} \\ \boldsymbol{D}_A = \boldsymbol{D}_B = \begin{bmatrix} 1 & -1 & 0 & \cdots & 0 \\ 1 & 0 & -1 & \cdots & 0 \\ \vdots & \vdots & \vdots & \vdots & \vdots \\ 1 & 0 & 0 & \cdots & -1 \end{bmatrix}_{n\times(n+1)} \end{cases} \tag{5}$$

where $\boldsymbol{O}$ is zero matrix.

$$\begin{cases} \lambda_j \Delta N_{br,j}^{s_B} - \lambda_i \Delta N_{br,i}^{1_A} = \lambda_j \Delta N_{br,j}^{s_B} - \lambda_j \Delta N_{br,i}^{1_A} + \lambda_j \Delta N_{br,i}^{1_A} - \lambda_i \Delta N_{br,i}^{1_A} \\ \qquad = \lambda_j \Delta \nabla N_{br,ij}^{1_A s_B} + \lambda_{ji} \Delta N_{br,i}^{1_A} \\ \Delta \nabla N_{br,ij}^{1_A s_B} = \Delta N_{br,j}^{s_B} - \Delta N_{br,j}^{1_B} + \Delta N_{br,j}^{1_B} - \Delta N_{br,i}^{1_A} = \Delta \nabla N_{br,ij}^{1_B s_B} + \Delta \nabla N_{br,ij}^{1_A 1_B} \\ \tilde{b}_{\mathrm{DISPB}} = b_{\mathrm{DISPB}} + \Delta \nabla N_{br,ij}^{1_A 1_B} + (\lambda_{ji}/\lambda_j) \cdot \Delta N_{br,i}^{1_A} \end{cases} \tag{7}$$

We assume that both systems A and B have n observable satellites in (5). It is used to convert the single difference ambiguity into the double difference ambiguity, and the converted double difference ambiguity is composed of the single difference ambiguities of two same systems, not of two different systems. This is the same as the traditional intra-system double difference RTK model. Compared with the traditional intra-system double difference model, this model adds the inter-system double difference observation equation. The addition of the inter-system double difference observation equation also introduces DISB parameter, not directly increasing the model strength. However, this model can use the time stability of ISBs and impose time constant constraints on ISBs by Kalman filter to improve the accuracy of the residual parameter solution. After using the Least Squares Ambiguity Decorrelation Adjustment (LAMBDA) (Teunissen, 1995) to fix the ambiguity, the high precision solution can be obtained by the following formula:

$$\hat{\boldsymbol{U}}_N = \tilde{\boldsymbol{U}}_N - \tilde{\boldsymbol{Q}}_{UN} \boldsymbol{Q}_N^{-1} (\hat{\boldsymbol{N}} - \tilde{\boldsymbol{N}}) \tag{6}$$

where $\hat{\boldsymbol{N}}$ and $\tilde{\boldsymbol{N}}$ represent the fixed and float solutions of the ambiguity parameter, respectively, $\hat{\boldsymbol{U}}_N$ and $\tilde{\boldsymbol{U}}_N$ represent the fixed and float solutions of the non-ambiguity parameter, respectively, and $\boldsymbol{Q}$ represents the covariance matrix.

However, since DISB is linearly dependent of the ambiguity parameter, using (6) can only obtain the ambiguity fixed solution for the coordinate parameters, not for DISB. This makes impossible to analyze the stability of DISB. To obtain the ambiguity fixed solution of DISPB parameters, we must reorganize the parameters to eliminate the linear correlation between DISB and ambiguity. The ambiguity and DISB parameters are reorganized as follows:

The state vector after parameter reorganization is represented as follows:

$$\begin{cases} \tilde{\boldsymbol{X}} = \left(\tilde{\boldsymbol{U}}_N \ \Delta \nabla N_{br,i}^{1_A s_A} \ \Delta \nabla N_{br,j}^{1_B s_B} \right) \\ \tilde{\boldsymbol{U}}_N = \left(x \, y \, z \, \tilde{b}_{\mathrm{DISCB}} \, b_{\mathrm{DISCB}} \right) \end{cases} \tag{8}$$

where $\tilde{\boldsymbol{U}}_N$ represents all the non-ambiguity parameters, including the coordinates and DISBs, and $\tilde{\boldsymbol{X}}$ contains the $\tilde{\boldsymbol{U}}_N$ and ambiguity parameters. Finally, we present the transformation matrix $\boldsymbol{F}$ from (4) to (8):

$$\begin{cases} \tilde{\boldsymbol{X}} = \boldsymbol{F}\boldsymbol{X} \\ \tilde{\boldsymbol{Q}}_{xx} = \boldsymbol{F}\boldsymbol{Q}_{xx}\boldsymbol{F}^{\mathrm{T}} \end{cases} \tag{9}$$

$$\boldsymbol{F} = \begin{bmatrix} \boldsymbol{I}_{3\times 3} & & & & \\ & 1_{\mathrm{DISPB}} & & \left\{-\lambda_i/\lambda_j\right\}_{RA} & 1_{RB} \\ & & 1_{\mathrm{DISCB}} & & \\ & & & \boldsymbol{D}_A & \\ & & & & \boldsymbol{D}_B \end{bmatrix} \tag{10}$$

where 1_{DISPB} represents the coefficient 1 corresponding to the state parameter DISPB, and $\left\{-\lambda_i/\lambda_j\right\}_{RA}$ represents

the coefficient $\{-\lambda_i/\lambda_j\}$ corresponding to single difference ambiguity of the reference satellite of system A.

Formula 5 can convert the single difference ambiguity without integer characteristics into the intra-system double difference ambiguity with integer characteristics. After fixing the ambiguity, (6) can be used to obtain the fixed solution for high precision coordinates. However, (5) eliminates the linear correlation between ambiguity parameters, but not between DISB and ambiguity parameters, so accurate DISB cannot be obtained. Through the derivation of formula (7), we can construct the transformation matrix (10). The transformation matrix (10) contains (5), which means that it eliminates the linear correlation not only between ambiguity parameters, but also between DISB and ambiguity. Thus, an absolute DISB can be obtained.

In summary, the Kalman filter is first used to obtain the float solution of (4), and the transition matrix (10) is subsequently used to convert the state vector (4) to (8), and the converted intra-system double difference ambiguity is fixed. After the ambiguity is fixed successfully, the accurate coordinates and DISB are obtained by (6).

Ionospheric-float inter-system double-differenced model

In a medium-long baseline, the ionospheric and tropospheric errors cannot be completely eliminated because the two stations are far apart (Li et al., 2015). The ionospheric-float single-differenced observation equations are formulated as follows:

$$\begin{cases} \Delta P_{br,i}^{s_A} = \Delta\rho_{br}^{s_A} + \Delta dt_{br} + \Delta d_{br,i}^{A} + \mu_i^{s_A} I_{br,i}^{s_A} + M_r^{s_A} T_r - M_b^{s_A} T_b + \Delta e \\ \Delta\varphi_{br,i}^{s_A} = \Delta\rho_{br}^{s_A} + \Delta \mathrm{d}t_{br} + \lambda_i\left(\Delta\Phi_{br,i} + \Delta\delta_{br,i}^{A} + \Delta N_{br,i}^{s_A}\right) - \mu_i^{s_A} I_{br,i}^{s_A} + M_r^{s_A} T_r - M_b^{s_A} T_b + \Delta\varepsilon \end{cases} \tag{11}$$

where $I_{br,i}^{s_A}$ represents single-difference ionospheric delay, T_r represents tropospheric Zenith Wet Delay (ZWD) for receiver r, $\mu_i^{s_A}$ is the frequency dependent ionospheric delay coefficient, and $M_b^{s_A}$ is the tropospheric mapping function.

Similarly, one satellite is selected from the multiple systems to form the double difference observation equations. The ionospheric-float inter-system double-difference observation equations are formulated as follows:

$$\begin{cases} \Delta\nabla P_{br,ij}^{1_A s_B} = \Delta\nabla\rho_{br}^{1_A s_B} + b_{\mathrm{DISCB}} + \mu_i^{1_A} I_{br,i}^{1_A} + \mu_j^{s_B} I_{br,j}^{s_B} + M_r^{1_A s_B} T_r - M_b^{1_A s_B} T_b + \Delta\nabla e \\ \Delta\nabla\varphi_{br,ij}^{1_A s_B} = \Delta\nabla\rho_{br}^{1_A s_B} + b_{\mathrm{DISPB}} + \lambda_j \Delta N_{br,j}^{s_B} - \lambda_i \Delta N_{br,i}^{1_A} - \mu_i^{1_A} I_{br,i}^{1_A} - \mu_j^{s_B} I_{br,j}^{s_A} + \\ \qquad M_r^{1_A s_B} T_r - M_b^{1_A s_B} T_b + \Delta\nabla\varepsilon \end{cases} \tag{12}$$

The state vector is as follows:

$$\boldsymbol{X} = \left(x\, y\, z\, I_{br,i}^{s_A}\, I_{br,j}^{s_B}\, T_r\, T_b\, b_{\mathrm{DISPB}}\, b_{\mathrm{DISCB}}\, \Delta N_{br,i}^{s_A}\, \Delta N_{br,j}^{s_B}\right) \tag{13}$$

Since the frequencies of satellites A and B may not be the same, the single-difference ionospheric delay is still estimated here. In this way, the destruction of the double difference ionospheric coefficient for non-overlapping frequencies can be avoided. Similar to the ionospheric-fixed inter-system double-differenced model, after the float solution of the state parameters is obtained with the Kalman filter, the F1 matrix is used for the transformation.

$$\boldsymbol{F}_1 = \begin{bmatrix} \boldsymbol{I}_{(2n+5)\times(2n+5)} & & & & \\ & 1_{\mathrm{DISPB}} & & \{\lambda_i/\lambda_j\}_{RA} & 1_{RB} \\ & & 1_{\mathrm{DISCB}} & & \\ & & & \boldsymbol{D}_A & \\ & & & & \boldsymbol{D}_B \end{bmatrix} \tag{14}$$

Similarly, after completing the transformation using the $\boldsymbol{F}_1$ matrix, the LAMBDA method can be used to obtain the fixed solution.

Experimental results

We first test the stability of DISB using the proposed model. The positioning performance of the proposed model is then tested on three baselines with different lengths. The dual-frequency observation data of GPS/BDS/Galileo are used in all the experiments, and the sampling interval is 30 s.

Experiments for the stability analysis of DISB

In this section, the stability of DISCB and DISPB is analyzed, including L1–B1 and L2–B2 of GPS/ BDS as well as L1–E1 and L2–E5a of GPS/Galileo. It is worth noting that among these frequencies, only L1-E1 are overlapping frequencies, and the others are all non-overlapping

Table 1 Information of baselines for analyzing the stability of DISB

Baseline	Receivers	Duration (h)	Length (m)
CUT0-CUT2	Trimble NETR9- Trimble NETR9	24	0
CUT0-CUT1	Trimble NETR9- SEPT POLARX4	24	0

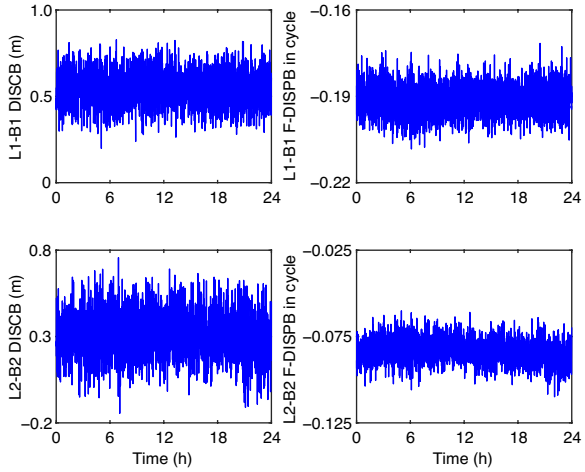

Fig. 1 DISB time series for L1-B1 and L2-B2 with same receiver types

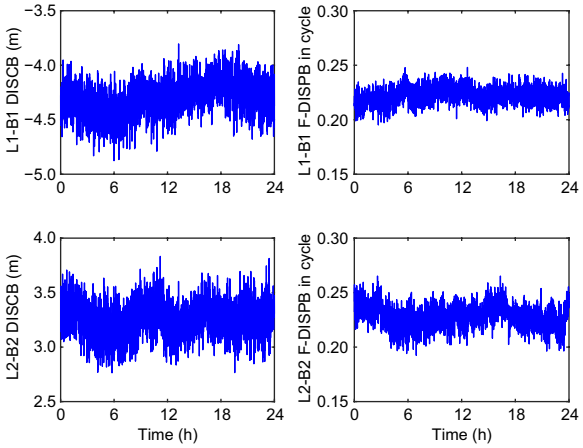

Fig. 3 DISB time series for L1-B1 and L2-B2 with different receiver types

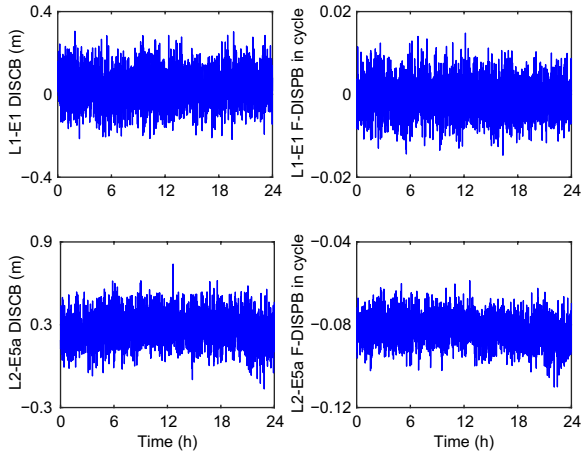

Fig. 2 DISB time series for L1-E1 and L2-E5a with same receiver types

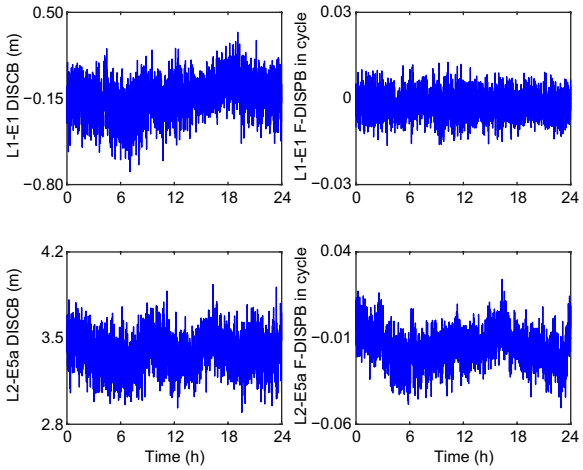

Fig. 4 DISB time series for L1-E1 and L2-E5a with different receiver types

frequencies. We used two sets of baseline data with the same and different types of receivers. The satellite cut-off elevation angle was set at 15 degrees. To obtain more accurate results, the single epoch model was used to estimate DISB (Gao et al., 2017).

Two sets of zero baseline data were used to test the stability of DISB. Their specific information is shown in Table 1. CUT0-CUT2 uses the same type of receiver, and CUT0-CUT1 uses different types of receivers.

Figures 1, 2, 3, and 4 illustrate the DISB time series for these two baselines. Their mean and STandard Deviations (STD) are in Table 2. Since the integer part of the DISPB is affected by the reference satellite transformation, we only focus on the fractional part of the DISPB (Shang et al., 2021a, 2021b).

Figures 1 and 2 illustrate the DISB time series of CUT0-CUT2. This is a baseline with the same type of receivers. As can be seen in Fig. 2, both DISCB and DISPB are close to 0 for overlapping frequencies. However, the DISBs for the non-overlapping frequencies are not close to zero and cannot be ignored. The DISB for both non-overlapping

Table 2 Mean and STD of DISB for the two baselines

Baseline	Frequency	Results of DISCB (m)		Results of DISPB in cycle	
		Mean	STD	Mean	STD
CUT0-CUT2	L1-B1	0.5436	0.0965	− 0.1914	0.0053
	L2-B2	0.3160	0.1249	− 0.0834	0.007
	L1-E1	0.0380	0.0861	− 0.0009	0.0044
	L2-E5a	0.2781	0.1115	− 0.0822	0.007
CUT0-CUT1	L1-B1	− 4.3046	0.1589	0.2222	0.0076
	L2-B2	3.2621	0.1607	0.2279	0.0107
	L1-E1	− 0.1451	0.1442	− 0.0021	0.0045
	L2-E5a	3.3844	0.1522	− 0.0156	0.0105

frequency and overlapping frequency has good stability with the same type of receiver used.

Figures 3 and 4 illustrate the DISB time series of CUT0-CUT1. This is a baseline with the different types of receivers. As can be seen from the figures, even for the overlapping frequency the DISB is not 0. Although the STD of DISB with different types of receivers are slightly larger than those with the same type, they are still within an admissible range. All in all, DISB has good stability regardless of the receiver type and the frequency of the signals used. In the multi-epoch positioning mode, the stability of DISB can be used to enhance the strength of the model and thus improve the positioning accuracy.

Experiments for positioning accuracy

In this section, the inter-system double-difference RTK model is tested using three baselines of different lengths and compared with the intra-system RTK model. The baselines information is in Table 3. All of them have a sampling interval of 30 s. GPS/BDS/Galileo dual frequency data was used in the three baselines. Ionospheric-fixed model is used to deal with the CUTB-CUTC baseline and ionospheric-float model is used to deal with the CUTB-PERT and CUTB-NNOR baselines. To further test the validity of the model, the satellites cut-off elevation angles were artificially set at 40 degrees to simulate a rare observation environment. Figure 5 presents the number of visible satellites for the three baselines.

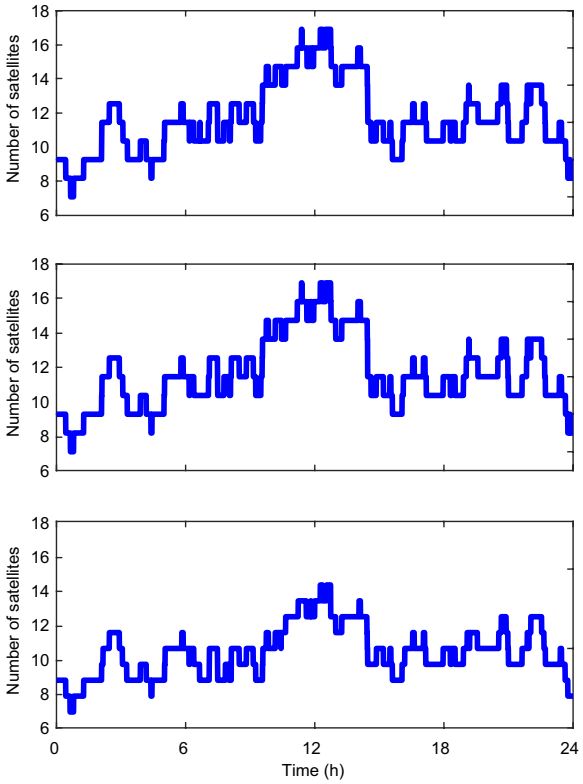

Fig. 5 The number of visible satellites for the three baselines

Figure 6 shows the positioning errors with the inter-system RTK model and the traditional intra-system RTK model in *E*, *N* and *U* directions for baseline CUTB-CUTC. The ambiguity fixed rates are 100% for both inter-system RTK model and the traditional intra-system RTK model. As can be seen from the figures, the inter-system RTK model gives higher positioning accuracy than intra-system RTK model. The Root Mean Square (RMS) of positioning errors obtained with these two methods are shown in Table 4. The RMSs of the positioning errors in *E*, *N* and *U* directions are 0.20 cm, 0.23 cm, and 0.93 cm for intra-system RTK model, and 0.18 cm, 0.18 cm, and 0.83 cm for inter-system RTK model, respectively.

Table 3 Information of three baselines with different lengths for positioning

Baseline	Receivers	Duration (h)	Length (km)
CUTB-CUTC	Trimble NETR9- Trimble NETR9	24	0
CUTB-PERT	Trimble NETR9- Trimble NETR9	24	22.4
CUTB-NNOR	Trimble NETR9-SEPT POLARX4	24	109.6

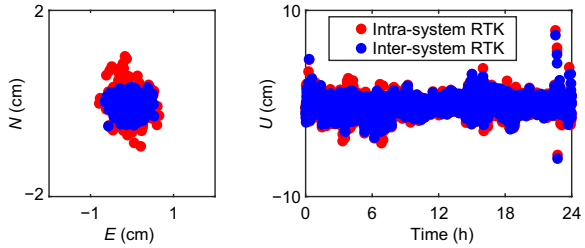

Fig. 6 Positioning errors with the inter-system RTK model and the traditional intra-system RTK model in *E*, *N* and *U* directions for CUTB-CUTC

Table 4 RMS of positioning errors with the inter-system RTK model and the traditional intra-system RTK model in east (*E*), north (*N*) and up (*U*) directions for CUTB-CUTC

Items	RMS in directions (cm)			Ambiguity fixed rate (%)
	E	*N*	*U*	
Intra-system RTK	0.2	0.23	0.93	100%
Inter-system RTK	0.18	0.18	0.83	100%
Improvement	10%	22%	11%	0

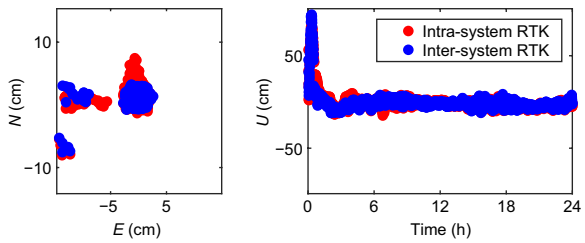

Fig. 7 Positioning errors of the inter-system RTK model and the traditional intra-system RTK model in *E*, *N* and *U* directions for CUTB-PERT

Table 5 RMS of positioning errors of the inter-system RTK model and the traditional intra-system RTK model in *E*, *N* and *U* directions for CUTB-PERT

Items	RMS in different directions (cm)			TTFF in epoch	Ambiguity fixed rate (%)
	E	*N*	*U*		
Intra-system RTK	3.35	1.40	13.6	66	96%
Inter-system RTK	3.14	1.25	12.61	46	97%
Improvement	6%	11%	7%	30%	1%

Compared with the intra-system RTK model, the positioning accuracy of the inter-system RTK model in *E*, *N* and *U* directions is improved by 10%, 22% and 11%, respectively. The ambiguity fixed rate is 100% for both inter-system RTK model and intra-system RTK model.

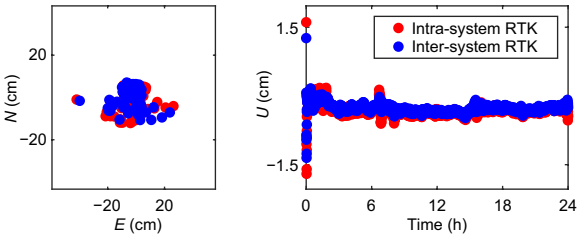

Fig. 8 Positioning errors of the inter-system RTK model and the traditional intra-system RTK model in *E*, *N* and *U* directions for CUTB-NNOR

Table 6 RMS of positioning errors of the inter-system RTK model and the traditional intra-system RTK model in *E*, *N* and *U* directions for CUTB-NNOR

Items	RMS in different directions (cm)			TTFF in epoch	Ambiguity fixed rate (%)
	E	*N*	*U*		
Intra-system RTK	2.33	2.02	12.28	221	91
Inter-system RTK	1.82	1.68	9.84	156	94
Improvement	22%	17%	20%	29%	3%

Figure 7 shows the positioning errors with the inter-system RTK model and the traditional intra-system RTK model in *E*, *N* and *U* directions for baseline CUTB-PERT. It is a medium-long baseline with a length of 22 km, which means that it is difficult to fix the ambiguity at the beginning. Even with our proposed inter-system RTK model, it also requires a certain convergence time. The RMSs of positioning errors are shown in Table 5, which also includes large errors that are converging. The RMSs of the positioning errors in *E*, *N* and *U* directions are 3.35 cm, 1.40 cm, and 13.6 cm for intra-system RTK model, and 3.14 cm, 1.25 cm, and 12.61 cm for inter-system RTK model, respectively. Compared with the intra-system RTK model, the positioning accuracy of the inter-system RTK model in *E*, *N* and *U* directions is improved by 6%, 11%, and 7%, respectively. In addition, we also counted the Time to First Fix (TTFF) of the two models. It is worth noting that only the time when the ambiguity is successfully fixed in 10 consecutive epochs is considered as the first fix. The intra-system RTK model and the inter-system RTK model reach the first fix at the 66th and 46th epoch, respectively. Compared with the intra-system RTK model, the TTFF of the inter-system RTK model is shortened by 30%. The ambiguity fixed rates of

intra-system RTK model and inter-system RTK model are 96% and 97%, respectively.

Figure 8 shows the positioning errors of the inter-system RTK model and the traditional intra-system RTK model in *E*, *N* and *U* directions for baseline CUTB-NNOR. It is a longer baseline, which means that it is more challenging to obtain accurate positioning results. Compared to the baseline CUTB-PERT, the baseline CUTB-NNOR requires a longer convergence time. The RMSs of positioning errors are shown in Table 6. The RMSs of the positioning errors in E, N, and U directions are 2.33 cm, 2.02 cm, and 12.28 cm for intra-system RTK model, and 1.82 cm, 1.68 cm, and 9.84 cm for inter-system RTK model, respectively. Compared with the intra-system RTK model, the positioning accuracy of the inter-system RTK model in *E*, *N* and *U* directions is improved by 22%, 17%, and 20%, respectively. The intra-system RTK model and the inter-system RTK model reach the first fix at the 221st and 156th epoch, respectively, which is longer compared to baseline CUTB-PERT. Compared with the intra-system RTK model, the TTFF of the inter-system RTK model is shortened by 29%. The ambiguity fixed rates of intra-system RTK model and inter-system RTK model are 91% and 94%, respectively.

Conclusions

In this study, we developed a new inter-system double difference RTK model with single difference ambiguity estimation that can be applied for both overlapping and non-overlapping signal frequencies. By estimating the single difference ambiguity, the model effectively avoids the DISB parameter discontinuity caused by the reference satellite transformation. Compared with the traditional non-overlapping frequency double difference model, it is not necessary to use the code observations to calculate the single difference ambiguity of the reference satellite in advance. We also present the ionospheric-float mode and the ionospheric-fixed mode of this model. This makes the model applicable not only to short baseline scenarios but also to medium-long baseline scenarios. Specifically, we use this model to analyze the stability of DISB as well as the positioning performance.

The stability of DISCB and DISPB is tested extensively with multi-frequency, multi-system, and multi-type receiver. The conclusion is that both DISCB and DISPB have good stability, regardless of the frequency of the signal and the type of the receiver used. This means that the positioning accuracy with this model can benefit from the stability of DISCB and DISPB, which is the key reason for analyzing the stability of DISCB and DISPB.

We compare our proposed inter-system double-difference RTK model with the traditional intra-system double-difference RTK model in terms of positioning accuracy using three baselines with different lengths. Benefiting from the stability of DISB, the proposed inter-system double-difference model can improve the positioning accuracy by 6–22% compared with the intra-system double-difference model. The positioning results in two medium-long baselines show that the TTFF of inter-system double-difference RTK model is shortened by 30% and 29%, respectively, compared with that of traditional intra-system double-difference RTK model.

Abbreviations

DISB	Differential inter-system biases
DISCB	Differential inter-system code biases
DISPB	Differential inter-system phase biases
TTFF	The time to first fix
GNSS	Global navigation satellite system
BDS	BeiDou navigation satellite system
GPS	Global positioning system
RMS	Root-mean-square
RTK	Real-time kinematic
ZWDs	Zenith wet delays
LAMBDA	Least squares ambiguity decorrelation adjustment
STD	Standard deviations

Acknowledgements

Many thanks are due to Curtin University and IGS for providing GNSS data. This work is funded by the National Key Research Program of China Collaborative Precision Positioning Project (No. 2016YFB0501900) and the National Natural Science Foundation of China (No. 41774017).

Author contributions

Conceptualization, WZ; Data curation, MG; Formal analysis, GL and MG; Methodology, WZ; Software, MG; Supervision, GL; Validation, BZ and ML; Visualization, BZ and SH; Writing original draft, WZ; Writing review & editing, WZ and GL. All authors read and approved the final manuscript.

Funding

This work was jointly supported by the National Key Research Program of China Collaborative Precision Positioning Project (No. 2016YFB0501900) and the National Natural Science Foundation of China (Grant No. 41774017).

Availability of data and materials

The datasets that support the findings of this research are available from the corresponding author upon reasonable request.

Competing interests

The authors declare no conflict of interest.

Received: 8 January 2023 Accepted: 14 June 2023
Published online: 14 August 2023

References

Ge, C., Li, B., Zhang, Z., & Liu, T. (2021). Integer ambiguity resolution and precise positioning for tight integration of BDS-3, GPS, GALILEO, and QZSS overlapping frequencies signals. *GPS Solutions, 26*, 26. https://doi.org/10.1007/s10291-021-01203-1

Gao, W., Gao, C., Pan, S., Meng, X., & Xia, Y. (2017). Inter-system differencing between GPS and BDS for medium-baseline RTK positioning. *Remote Sensing*. https://doi.org/10.3390/rs9090948

Gao, W., Meng, X., Gao, C., Pan, S., & Wang, D. (2018). Combined GPS and BDS for single-frequency continuous RTK positioning through real-time estimation of differential inter-system biases. *GPS Solutions*. https://doi.org/10.1007/s10291-017-0687-5

Jia, C., Zhao, L., Li, L., Gao, Y., & Gao, Y. (2019). Pivot single-difference ambiguity resolution for multi-GNSS positioning with non-overlapping frequencies. *GPS Solutions, 23*, 97. https://doi.org/10.1007/s10291-019-0891-6
Khodabandeh, A., & Teunissen, P. J. G. (2016). PPP-RTK and inter-system biases: The ISB look-up table as a means to support multi-system PPP-RTK. *Journal of Geodesy, 90*(9), 837–851.
Li, B., Feng, Y., Gao, W., & Li, Z. (2015). Real-time kinematic positioning over long baselines using triple-frequency BeiDou signals. *IEEE Transactions on Aerospace and Electronic Systems, 51*, 3254–3269. https://doi.org/10.1109/TAES.2015.140643
Mi, X., Zhang, B., & Yuan, Y. (2019). Multi-GNSS inter-system biases: Estimability analysis and impact on RTK positioning. *GPS Solutions*. https://doi.org/10.1007/s10291-019-0873-8
Odijk, D., et al. (2016). On the estimability of parameters in undifferenced, uncombined GNSS network and PPP-RTK user models by means of S-system theory. *Journal of Geodesy, 90*(1), 15–44.
Odijk, D., & Teunissen, P. J. G. (2013). Characterization of between-receiver GPS-Galileo inter-system biases and their effect on mixed ambiguity resolution. *GPS Solutions, 17*, 521–533. https://doi.org/10.1007/s10291-012-0298-0
Odolinski, R., & Teunissen, P. J. G. (2020). Best integer equivariant estimation: Performance analysis using real data collected by low-cost, single- and dual-frequency, multi-GNSS receivers for short- to long-baseline RTK positioning. *Journal of Geodesy, 94*, 91. https://doi.org/10.1007/s00190-020-01423-2
Odolinski, R., Teunissen, P. J. G., & Odijk, D. (2014). First combined COMPASS/BeiDou-2 and GPS positioning results in Australia. Part II: Single- and multiple-frequency single-baseline RTK positioning. *Journal of Spatial Science, 59*, 25–46. https://doi.org/10.1080/14498596.2013.866913
Paziewski, J., & Wielgosz, P. (2015). Accounting for Galileo–GPS inter-system biases in precise satellite positioning. *Journal of Geodesy, 89*, 81–93. https://doi.org/10.1007/s00190-014-0763-3
Shang, R., Gao, C., Gao, W., Zhang, R., Peng, Z., & Liu, Q. (2021). Multi-GNSS inter-system model for complex environments based on optimal state estimation. *Measurement Science and Technology, 32*, 054006. https://doi.org/10.1088/1361-6501/abdae5
Shang, R., Gao, C. F., Gao, W., Zhang, R. C., & Peng, Z. H. (2021). A single difference-based multi-GNSS inter-system model with consideration of inter-frequency bias and inter-system bias. *Measurement Science and Technology*. https://doi.org/10.1088/1361-6501/abbf0d
Sui, X. (2018). Research on the theory and method of inter-system double difference ambiguity forming and fixing for multi-GNSS. *Acta Geodetica et Cartographica Sinica, 47*, 1160–1160.
Takasu, T., & Yasuda, A. (2009). Development of the low-cost RTK-GPS receiver with an open source program package RTKLIB. In *International Symposium on GPS/GNSS*.
Tao, J., Chen, G., Guo, J., Zhang, Q., Liu, S., & Zhao, Q. (2022). Toward BDS/Galileo/GPS/QZSS triple-frequency PPP instantaneous integer ambiguity resolutions without atmosphere corrections. *GPS Solutions, 26*, 127. https://doi.org/10.1007/s10291-022-01287-3
Teunissen, P. J. G. (1995). The least-squares ambiguity decorrelation adjustment: A method for fast GPS integer ambiguity estimation. *Journal of Geodesy, 70*, 65–82. https://doi.org/10.1007/BF00863419
Teunissen, P. J. G., & Khodabandeh, A. (2022). PPP–RTK theory for varying transmitter frequencies with satellite and terrestrial positioning applications. *Journal of Geodesy, 96*, 84. https://doi.org/10.1007/s00190-022-01665-2
Tian, Y., Ge, M., Neitzel, F., & Zhu, J. (2017). Particle filter-based estimation of inter-system phase bias for real-time integer ambiguity resolution. *GPS Solutions, 21*, 949–961. https://doi.org/10.1007/s10291-016-0584-3
Tian, Y., Liu, Z., Ge, M., & Neitzel, F. (2018). Determining inter-system bias of GNSS signals with narrowly spaced frequencies for GNSS positioning. *Journal of Geodesy, 92*, 873–887. https://doi.org/10.1007/s00190-017-1100-4
Wu, M., Zhang, X., Liu, W., Wu, R., Zhang, R., Le, Y., & Wu, Y. (2018). Influencing factors of GNSS differential inter-system bias and performance assessment of tightly combined GPS, Galileo, and QZSS relative positioning for short baseline. *Journal of Navigation, 72*, 1–22. https://doi.org/10.1017/S0373463318001017
Wu, Z., Wang, Q., Yu, Z., Hu, C., Liu, H., & Han, S. (2022). Modeling and performance assessment of precise point positioning with multi-frequency GNSS signals. *Measurement, 201*, 111687. https://doi.org/10.1016/j.measurement.2022.111687
Xiao, G., Liu, G., Ou, J., Liu, G., Wang, S., & Guo, A. (2020). MG-APP: An open-source software for multi-GNSS precise point positioning and application analysis. *GPS Solutions, 24*, 66. https://doi.org/10.1007/s10291-020-00976-1
Zhao, W., Liu, G., Gao, M., Lv, D., & Wang, R. (2022). INS-assisted inter-system biases estimation and inter-system ambiguity resolution in a complex environment. *GPS Solutions, 27*, 3. https://doi.org/10.1007/s10291-022-01347-8
Zhao, W. H., Liu, G. Y., Wang, S. L., Gao, M., & Lv, D. (2021). Real-time estimation of GPS-BDS inter-system biases: An improved particle swarm optimization algorithm. *Remote Sensing*. https://doi.org/10.3390/rs13163214

Publisher's Note